Indian Journal of Chemistry
Vol. 55A, February 2016, pp. 145-152

Synthesis of zinc porphyrins and effect of peripheral substituents on the coordination reaction

Shujun Wang*, Yuling Peng, Chenggen Zhang, Yongbing Li & Chao Liu
College of Chemistry and Materials Science, Langfang Teachers University, Langfang 065000, China
Email: d022036@mail.nankai.edu.cn

Received 28 August 2015; revised and accepted 22 January 2016

Three free-base porphyrins, modified with Boc-D-threonine and their zinc porphyrins have been synthesized using benzaldehyde, 4-chlorobenzaldehyde, and 4-methoxybenzaldehyde. The effects of peripheral substituents on the coordination reactions between zinc porphyrins and imidazole derivatives have been studied by UV-visible spectroscopy, fluorescence spectrometry, and theoretical calculations. The results show that the coordination reaction forms a Zn-N bond between zinc porphyrins involving different peripheral substituents and imidazole derivatives. The association coordination constants decrease (N-MeIm > Im) due to the change in enthalpy; the zinc porphyrin synthesized using 4-chlorobenzaldehyde and N-methylimidazole shows the largest association constant. Fluorescent quenching is observed during the coordination process with the zinc porphyrin synthesized using 4-methoxybenzaldehyde and N-methylimidazole showing the largest Stern-Volmer quenching rate constant. In addition, theoretical calculations have been used to investigate essential characteristics of the reaction, charges, bond lengths, and bond energies for each system.

Keywords: Coordination chemistry, Theoretical chemistry, Porphyrins, Zinc porphyrins, UV-visible spectroscopy, Fluorescence quenching

Porphyrins are macromolecular heterocyclic compounds formed by α-carbon atoms in four pyrrole subunits via methylene bridge (=CH-) interconnections; these compounds can combine with metal ions to form metal porphyrins. There are several examples of naturally occurring metal porphyrins with important physiological functions, including heme, an iron porphyrin, chlorophyll, a magnesium porphyrin, and vitamin B_{12}, a cobalt porphyrin. Porphyrin is often employed in reaction models of hemoglobin, myoglobin, cytochrome *c*, and other biological molecules[1-23]. For example, the axial coordination reaction between porphyrin and a small molecule containing a nitrogen atom has been widely used in molecular devices designed for energy and electron transfer, multi-redox catalysis, sensors, and molecular recognition[24-28].

Imidazole derivatives with similar structures as natural enzyme ligands are common electron donors in coordination reactions. When imidazole derivatives are coordinated with a metal porphyrin, they play an important role in electron transfer, improving electro-optical properties, and stabilizing systems[29,30].

Threonine is an amino acid with important biological functions. For example, certain protein kinases that include threonine have antiviral activity, which was studied by Venditto[31] and Darbinian[32]. Thus, this amino acid could provide a new path for drug development. If threonine was anchored to porphyrin, the biological activities of these molecules could be combined, thus altering the photoelectric properties and biological activities of porphyrins.

Herein, we have utilized Boc-D-threonine to synthesize three free-base porphyrins and their respective zinc porphyrins. We have studied the coordination reactions between zinc porphyrins and different substituted groups and imidazole derivatives by using ultraviolet-visible (UV-vis) spectroscopy, quantum chemistry, and fluorescence spectroscopy. Thermodynamic parameters were determined using the van't Hoff equation, and fluorescence quenching data were analyzed using the Stern-Volmer equation. The charges, bond lengths, and bond energies for each coordination system were obtained by theoretical calculations. These experimental results contribute to a variety of areas, including drug design, protein engineering, and gene technology.

Materials and Methods

The percentage of C, H, and N content was determined using an EAI CE-440 elemental analyzer. ^{1}H nuclear magnetic resonance (NMR) was recorded

on a Bruker 400 MHz spectrometer ($CDCl_3$, TMS). UV-vis spectra were obtained using a Shimadzu-2550 spectrometer. The fluorescence measurements were made using an F-4600 fluorescence spectrometer.

Pyrrole and *N*-methylimidazole (*N*-MeIm) were distilled, while *p*-nitrobenzaldehyde and imidazole (Im), were recrystallized from water and ethanol respectively. Boc-D-threonine, a biochemical reagent, was purchased from Beijing J&K Technology Co., Ltd. (Beijing, China). Dry CH_2Cl_2 was obtained by redistillation from $CaCl_2$. Other reagents were commercial chemicals of analytical grade that were used as received, without further purification.

Spectral studies

A stock solution of Im and *N*-MeIm was added to 2.5 μ*M* zinc porphyrin in CH_2Cl_2, and the change in absorption at the Soret band was monitored at 5, 10, 15, and 20 °C.

The n value and K^{θ} were given by Eq. (1). The thermodynamic parameters, $\Delta_r H^{\theta}_m$ and $\Delta_r S^{\theta}_m$, were determined using the van't Hoff equation (Eq. 2). The free energy value, $\Delta_r G^{\theta}_m$, was calculated using Eq. (3)[33-35].

$$\ln\frac{(A_o - A_e)}{(A_e - A_\infty)} = n\ln c_L + \ln K^{\theta} \quad \ldots(1)$$

$$\ln K^{\theta} = -\frac{\Delta_r H^{\theta}_m}{RT} + \frac{\Delta_r S^{\theta}_m}{R} \quad \ldots(2)$$

$$\Delta_r G^{\theta}_m = \Delta_r H^{\theta}_m - T\Delta_r S^{\theta}_m \quad \ldots(3)$$

To record the fluorescence spectrum, a stock solution of Im and *N*-MeIm was added to 2.5 μ*M* zinc porphyrin in CH_2Cl_2 at room temperature. The excitation and emission bandwidths were all obtained at 10 nm. The excitation wavelength was 420 nm. The Stern-Volmer quenching constant, K_{sv} (L mol^{-1}), was calculated using Eq. (4)[36].

$$\frac{F_o}{F} = 1 + K_q\tau_o[Q] = 1 + K_{sv}[Q] \quad \ldots(4)$$

Theoretical calculations

All standard density functional theory calculations were carried out using the Gaussian 09 program[37-39]. All structures were optimized at the B3LYP/BS level. BS denotes a basis set combining LANL2DZ for Zn and 6-31+G(d) for non-metal atoms. Harmonic frequency analysis calculations were performed to characterize the optimized structures to be minimal (no imaginary frequency).

Synthesis of the zinc porphyrins

The synthetic route for the three zinc porphyrins is shown in Scheme 1.

1a: A mixture of 4-nitrobenzaldehyde (2.57 g, 0.017 mol), benzaldehyde (5.41 g, 0.051 mol), and pyrrole (0.536 g, 8 mmol) in 120 mL of CH_3CH_2COOH was stirred and heated to reflux for 5 min. After the addition of pyrrole (4.29 g, 0.064 mol) dissolved in 25 mL of CH_3CH_2COOH, the reaction mixture was stirred for an additional 20 min. The mixture was refluxed under microwave conditions for 2 min and allowed to cool overnight. The CH_3CH_2COOH was distilled under reduced pressure. The total crude material was a purple powder.

1b was synthesized as described for **1a**, except that benzaldehyde was replaced by 4-chlorobenzaldehyde.

1c: A mixture of 4-nitrobenzaldehyde (0.6 g, 4 mmol), 4-methoxybenzaldehyde (1 mL, 0.051 mol), and pyrrole (0.85 mL, 8 mmol) in 12 mL of acetic anhydride was stirred and added to 100 mL of glacial acetic acid. The mixture was refluxed for 60 min. The mixture was allowed to cool and extracted. The total crude material was a purple powder.

2a: Crude **1a** (30 mg) was dissolved in 80 mL of concentrated hydrochloric acid. Stannous chloride dihydrate (2.6 g) was added to the solution and the reaction was heated to 65-70 °C for 1.5 h. The solution was cooled and added to 100 mL of water and the *p*H was adjusted to 8 using concentrated ammonium hydroxide. The aqueous phase was extracted with chloroform. The organic phase was concentrated on a rotary evaporator to 50 mL, and this was chromatographed through a silica column with chloroform as the eluent. The second band to elute from the column was the desired compound. Yield: 18.4%.

2b was prepared as described for **2a**, using **1b** as the starting material. Yield: 21.2%.

2c was prepared as described for **2a**, using **1c** as the starting material. Yield: 15.3%.

3a: An excess of Boc-D-threonine (20 mg, 0.11 mmol) was added to a solution of **2a** (100 mg, 0.074 mmol) in CH_2Cl_2 (60 mL), and the mixture was stirred in an ice bath for 10 min. To this solution, N,N′-dicyclohexylcarbodiimide was added dropwise over 20 min, with stirring for an additional 12 h. The ice bath was removed and the mixture was washed with 10% aqueous Na_2CO_3 and water, prior to drying

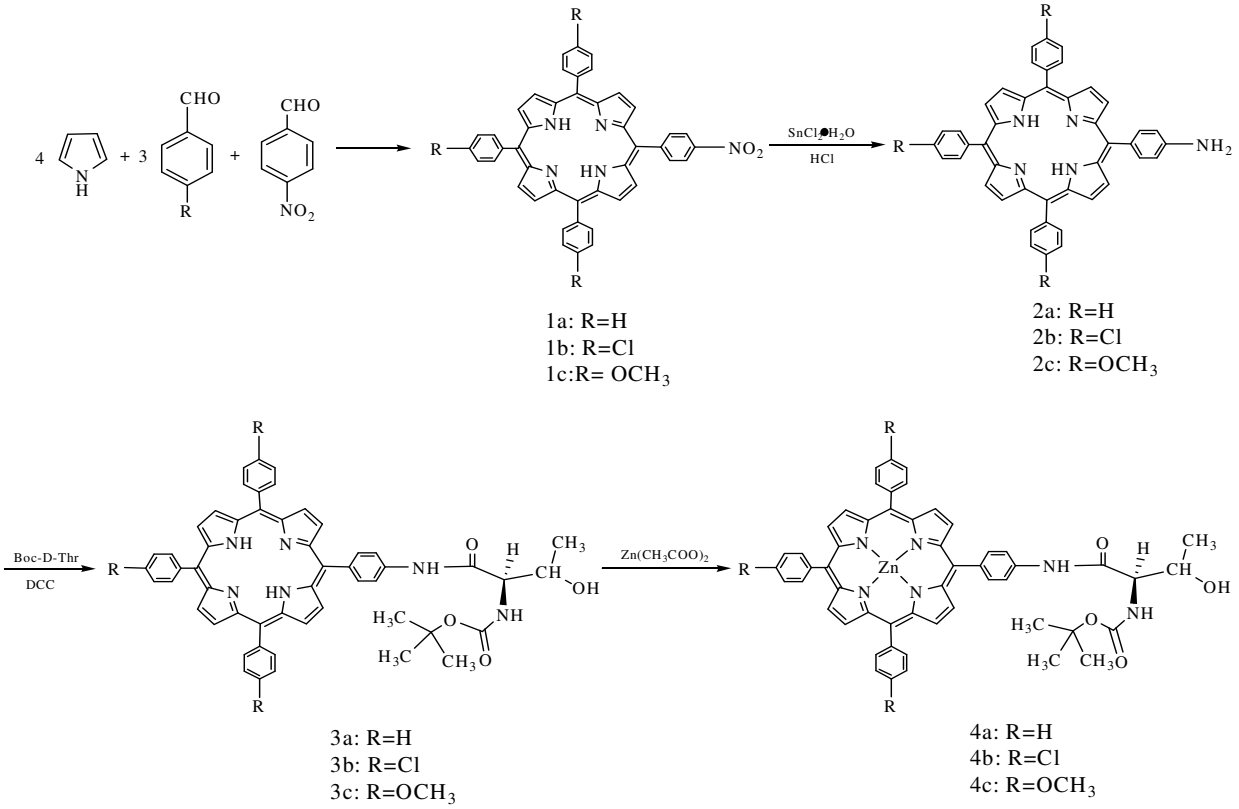

Synthetic route of zinc porphyrins

Scheme 1

over Na_2SO_4. The resulting solid was dissolved in $CHCl_3$ and then purified on a silica gel column. The red band was collected as the product, with a yield of 72.3%. Anal. (%): Calcd for $C_{53}H_{46}O_4N_6$: C, 76.63; H, 5.54; N, 10.12. Found: C, 76.88; H, 5.88; N, 9.84. ^{1}H NMR ($CDCl_3$, 400 Hz): δ: 8.839–8.853 (t, 8H, pyrrole H), 8.177–8.221 (m, 8H, 5, 10, 15, 20 Ar-*o*-H), 7.892 (d, 2H, 5 Ar-*m*-H), 7.732–7.784 (m, 9H, 10, 15, 20 Ar-*m*-H and *p*-H), 5.735 (d, 1H, CO-NH), 4.691 (d, 1H, α H), 4.338 (d, 1H, β H), 3.291 (s, 1H, ArNH), 1.577 (s, 9H, $C(CH_3)_3$), 1.364-1.384 (t, 3H, CH_3), –2.785 ppm (s, 2H, pyrrole NH).

3b was prepared as described for **3a**, using **2b** as the starting material. Yield: 78.3%. Anal. (%): Calcd for $C_{53}H_{43}O_4N_6Cl_3$: C, 68.13; H, 4.61; N, 9.00. Found: C, 67.88; H, 4.98; N, 9.25. ^{1}H NMR ($CDCl_3$, 400 Hz): δ: 8.814–8.874 (m, 8H, pyrrole-H), 8.118–8.183 (m, 8H, 5, 10, 15, 20 Ar-*o*-H), 7.921 (d, 2H, 5 Ar-*m*-H), 7.731–7.759 (m, 6H, 10, 15, 20 Ar-*m*-H), 5.742 (d, 1H, CO-NH), 4.676 (s, 1H, α H), 4.335-4.351 (m, 1H, β H), 3.286 (s, 1H, ArNH), 1.679 (s, 9H, $C(CH_3)_3$), 1.473 (d, 3H, CH_3), –2.849 ppm (s, 2H, pyrrole NH).

3c was prepared as described for **3a**, using **2c** as the starting material. Yield: 68.4%. Anal. (%): Calcd for $C_{56}H_{52}O_7N_6$: C, 73.04; H, 5.65; N, 9.13. Found: C, 72.88; H, 5.98; N, 9.44. ^{1}H NMR ($CDCl_3$, 400 Hz): δ: 8.845–8.865 (m, 8H, pyrrole-H), 8.110–8.194 (m, 8H, 5, 10, 15, 20 Ar-*o*-H), 7.871–7.921 (t, 2H, 5 Ar-*m*-H), 7.289 (d, 6H, 10, 15, 20 Ar-*m*-H), 5.750 (d, 1H, CO-NH), 4.687 (s, 1H, α H), 4.355 (d, 1H, β H), 4.102 (s, 9H, OCH_3), 3.487 (d, 1H, ArNH), 1.679 (s, 9H, $C(CH_3)_3$), 1.445 (d, 3H, CH_3), –2.765 ppm (s, 2H, pyrrole NH).

4a: An excess of $Zn(OAc)_2{\cdot}2H_2O$ (20 mg, 0.11 mmol) was added to a solution of **3a** (100 mg, 0.074 mmol) in CH_2Cl_2-MeOH (20 mL, 10:1), and the mixture was refluxed in the absence of light for 1 h. After refluxation, the solution was washed with H_2O and dried over Na_2SO_4. The contents were filtered, the mixture was evaporated to dryness, and the remaining material was purified on a silica gel column (20:1 $CHCl_3$/ether as eluent) to obtain the product, a red amorphous solid. Yield: 88.5%. Anal. (%): Calcd for $C_{53}H_{44}O_4N_6Zn$: C, 71.22; H, 4.93; N, 9.41. Found: C, 71.65; H, 5.18; N, 9.05. ^{1}H NMR ($CDCl_3$, 400 Hz):

δ: 8.944–8.970 (m, 8H, pyrrole H), 8.181–8.226 (m, 8H, 5, 10, 15, 20 Ar-*o*-H), 7.904 (d, 2H, 5 Ar-*m*-H), 7.731–7.782 (m, 9H, 10, 15, 20 Ar-*m*-H and *p*-H), 5.738 (d, 1H, CO-NH), 4.703 (d, 1H, α H), 4.302 (d, 1H, β H), 3.283 (s, 1H, ArNH), 1.569 (s, 9H, $C(CH_3)_3$), 1.445-1.487 (t, 3H, CH_3).

4b was prepared as described for **4a**, using **3b** as the starting material. Yield: 91.7%. Anal. (%): Calcd for $C_{53}H_{41}O_4N_6Cl_3Zn$: C, 63.82; H, 4.11; N, 8.43. Found: C, 63.58; H, 4.54; N, 8.71. ^{1}H NMR ($CDCl_3$, 400 Hz): δ: 8.917–8.984 (m, 8H, pyrrole-H), 8.126–8.181 (m, 8H, 5, 10, 15, 20 Ar-*o*-H), 7.902 (d, 2H, 5 Ar-*m*-H), 7.730–7.751 (t, 6H, 10, 15, 20 Ar-*m*-H), 5.698 (d, 1H, CO-NH), 4.616 (s, 1H, α H), 4.295 (d, 1H, β H), 3.240 (s, 1H, ArNH), 1.562 (s, 9H, $C(CH_3)_3$), 1.427-1.449 (d, 3H, CH_3).

4c was prepared as described for **4a**, using **3c** as the starting material. Yield: 84.1%. Anal. (%): Calcd for $C_{56}H_{50}O_7N_6Zn$: C, 68.36; H, 5.09; N, 8.55. Found: C, 68.72; H, 5.18; N, 8.14. ^{1}H NMR ($CDCl_3$, 400 Hz): δ: 8.969–8.998 (m, 8H, pyrrole-H), 8.109–8.166 (m, 8H, 5, 10, 15, 20 Ar-*o*-H), 7.905 (d, 2H, 5 Ar-*m*-H), 7.279-7.301 (t, 6H, 10, 15, 20 Ar-*m*-H), 5.743 (d, 1H, CO-NH), 4.636 (s, 1H, α H), 4.322 (d, 1H, β H), 4.106 (s, 9H, OCH_3), 3.387 (s, 1H, ArNH), 1.674 (s, 9H, $C(CH_3)_3$), 1.444 (d, 3H, CH_3).

Results and Discussion

Spectral studies

Free-base porphyrins had four Q bands and one Soret band, whereas zinc porphyrins had two Q bands and one Soret band. Figure 1 shows the UV-vis spectra of the free-base porphyrins **3a** (curves 1 and 1'), **3b** (cures 2 and 2'), and **3c** (curves 3 and 3'). The structures of these porphyrins can be explained in terms of two groups of electron transitions[40]. S_0 (the ground state)→S_1 (the lowest singlet excited state transition) gives rise to the weak Q bands in the visible region, whereas S_0→S_2 (the lowest singlet excited states transition) produces the strong Soret band in the near-UV region. Figure 2 shows the UV-vis spectra of the zinc porphyrins, **4a** (curves 1 and 1'), **4b** (curves 2 and 2'), and **4c** (curves 3 and 3'). Fewer Q bands were observed, as compared with free-base porphyrins, and the zinc porphyrin Soret band was red-shifted because the molecular symmetry was changed by zinc ion coordination with the porphyrin ring. These spectral changes are spectroscopic properties of porphyrins.

^{1}H NMR spectra

The ^{1}H NMR spectra for **3a-3c** and **4a-4c** show the H chemical shift of the Boc-amino acid in **3a-3c**, confirming that the Boc-amino acid has reacted with **2a-2c**. The chemical shifts of the two protons inside the porphyrin ring in **3a-3c** were –2.785, –2.849, and –2.765 ppm, respectively. This peak disappeared in **4a-4c**, confirming the formation of zinc porphyrins.

Determination of binding constants

The isosbestic point

We measured the isosbestic point diagrams between **4a-4c** with Im and *N*-MeIm in the Soret band[1,28,29]. For example, when Im or *N*-MeIm was added to solutions of **4a**, the absorption intensity of

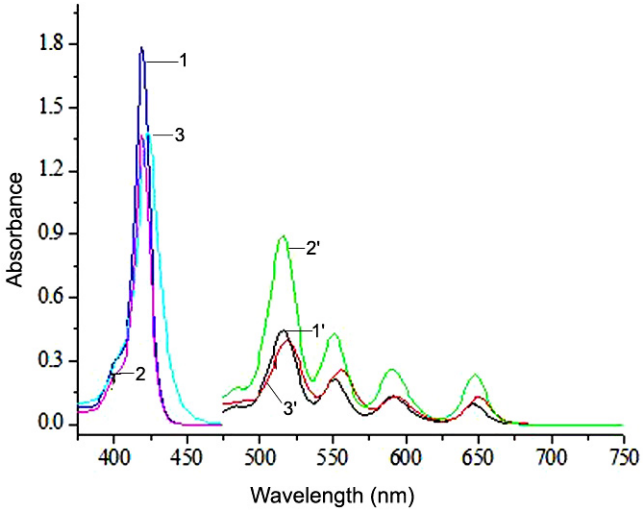

Fig. 1—UV-vis spectra of free porphyrins, **3a, 3b** and **3c**. [Curves 1, 2, and 3 are Soret bands of **3a, 3b** and **3c** respectively. Curves 1', 2', and 3' are Q bands of **3a, 3b** and **3c** respectively].

Fig. 2—UV-vis spectra of zinc porphyrins, **4a, 4b** and **4c**. [Curves 1, 2, and 3 are Soret bands of **4a, 4b** and **4c** respectively. Curves 1', 2', and 3' are Q bands of **4a, 4b** and **4c** respectively].

4a gradually weakened, the absorption intensity of the product gradually increased, and the clear isosbestic points of the porphyrin **4a**-Im or **4a**-*N*-MeIm systems were observed at 424.7 or 425.4 nm respectively (Fig. 3). Similar spectral changes were also observed for the **4b**-Im, **4b**-*N*-MeIm, **4c**-Im, and **4c**-*N*-MeIm systems. These changes in the curves are consistent with previously published findings[25,26]. The formation of an isosbestic point is a spectral characteristic of the axial coordination reaction.

The n value and association constants K^o

The n value and association constants K^o were calculated by plotting $\ln[(A_0-A_e)/(A_e-A_\infty)]$ $\ln c_L$ at four different temperatures (Eq. 1). The results showed that the n values were all close to 1 at different temperatures, indicating the formation of a 1:1 complex between zinc porphyrin and the imidazole derivatives. Apart from the 4 N atoms of the porphyrin ring, Zn^{2+} ion is also coordinated with an imidazole derivative. Thus, imidazole derivatives coordinated to the zinc porphyrin via a Zn-N bond, and five coordination systems were formed.

Using Eq. (2), the values of the association constants K^o were calculated and are listed in Table 1. As shown in Table 1, with the same porphyrin and imidazole derivatives, K^o decreased with increasing temperature, illustrating that the increased temperature did not promote this reaction. However, when the same porphyrin was used with a different imidazole derivative, the value of K^o decreased in the order of *N*-MeIm > Im. This is probably due to a methyl group belonging to the electron-donating group in *N*-MeIm, which is located at the *meta*-position of the coordinating nitrogen atoms. This group probably increased the charge density of the coordinating nitrogen atom, leading to a stronger

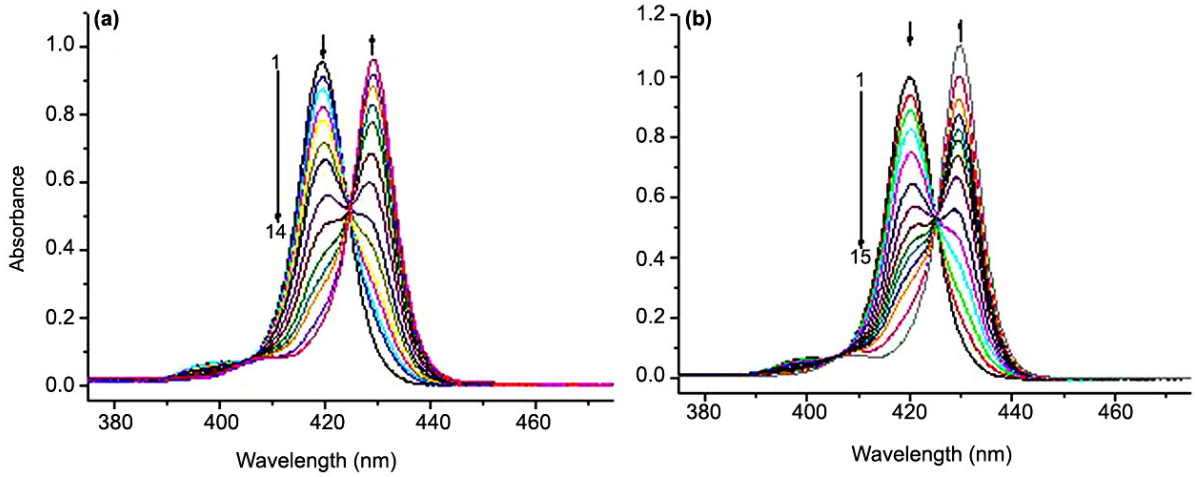

Fig. 3—The isosbestic points of the porphyrin **4a**-Im and **4a**-*N*-MeIm systems. [The arrows indicate increase or decrease of band intensity. (a) **4a**-Im system at 20 °C (curve 1: 4a, 2.5×10^{-6} mol L^{-1}; curves 2-14: $c_{Im}:c_{4a}$ = 3, 4, 5, 6, 8, 10, 15, 20, 30, 40, 50, 100, 200). (b) **4a**-*N*-MeIm system at 5 °C (curve 1: 4a, 2.5×10^{-6} mol L^{-1}; curves 2-15: $c_{N\text{-MeIm}}:c_{4a}$=0.4, 0.6, 1, 1.4, 2.4, 3, 4, 5, 6, 8, 10, 20, 30, 100)].

Table 1—The association constants (K^o) of the coordination reactions

System	K^o (L mol^{-1})			
	278 K	283 K	288 K	293 K
4a-Im	$(1.23\pm0.02)\times10^5$ (r = 0.9989)	$(8.13\pm0.01)\times10^4$ (r = 0.9989)	$(5.92\pm0.02)\times10^4$ (r = 0.9994)	$(4.28\pm0.01)\times10^4$ (r = 0.9993)
4a-*N*-MeIm	$(5.03\pm0.03)\times10^5$ (r = 0.9989)	$(3.33\pm0.02)\times10^5$ (r = 0.9989)	$(2.21\pm0.03)\times10^5$ (r = 0.9992)	$(1.52\pm0.02)\times10^5$ (r = 0.9990)
4b-Im	$(2.60\pm0.04)\times10^5$ (r = 0.9992)	$(1.77\pm0.02)\times10^5$ (r = 0.9992)	$(1.18\pm0.03)\times10^5$ (r = 0.9992)	$(8.16\pm0.04)\times10^4$ (r = 0.9995)
4b-*N*-MeIm	$(8.96\pm0.03)\times10^5$ (r = 0.9997)	$(5.73\pm0.04)\times10^5$ (r = 0.9995)	$(3.36\pm0.01)\times10^5$ (r = 0.9994)	$(2.24\pm0.02)\times10^5$ (r = 0.9994)
4c-Im	$(1.00\pm0.05)\times10^5$ (r = 0.9990)	$(7.68\pm0.01)\times10^4$ (r = 0.9991)	$(5.82\pm0.05)\times10^4$ (r = 0.9991)	$(4.44\pm0.03)\times10^4$ (r = 0.9992)
4c-*N*-MeIm	$(2.04\pm0.04)\times10^5$ (r = 0.9992)	$(1.48\pm0.02)\times10^5$ (r = 0.9990)	$(1.12\pm0.03)\times10^5$ (r = 0.9994)	$(8.61\pm0.04)\times10^4$ (r = 0.9990)

coordination with *N*-MeIm. Finally, for different porphyrins with the same imidazole derivatives, the **4b**-imidazole derivative system had the best association constant. This is because the chloride atom in **4b** is an electron-withdrawing group which increased the electropositivity of the zinc ions in the porphyrin plane, thereby enhancing the coordination ability of **4b**. In contrast, the methoxy group in **4c** is an electron-donating group that decreased the electropositivity of the zinc ions in the porphyrin plane, thereby weakening the coordination ability of **4c**. In summary, the system using **4b**-*N*-MeIm had the greatest association constant.

Thermodynamic parameters

Using Eq. (3), the values of the thermodynamic parameters, $\Delta_r G^{\ominus}_m$, $\Delta_r H^{\ominus}_m$, and $\Delta_r S^{\ominus}_m$, were calculated and are listed in Table 2. These data reveal the stability of each system. The $\Delta_r G^{\ominus}_m$ values showed that the formation of the reaction system was spontaneous. Furthermore, the value of $-\Delta_r H^{\ominus}_m$ was larger than that of $-\Delta_r S^{\ominus}_m$ for each system, indicating that the enthalpy change was the main driving force. These enthalpy changes may be ascribed to the electron transfer between the zinc and nitrogen atom. The entropy was negative, indicating that when imidazole derivatives interacted with zinc porphyrin, the two compounds generated a complex that restricted translational, rotational, and internal rotational motion[41]. The most negative values of $\Delta_r G^{\ominus}_m$ and $\Delta_r H^{\ominus}_m$ were observed for the **4b**-*N*-MeIm system, indicating the strongest interaction.

Theoretical calculations

In order to obtain the theoretical data relating to the coordination reaction, the geometry and electron structures of all systems were optimized at the B3LYP/6-31G* level. Table 3 presents the charges on the Zn atoms, Zn-N bond lengths, and bond energies for each system.

Table 2—Thermodynamic data of the coordination reactions

Systems	$\Delta_r H^{\ominus}_m$ (kJ mol^{-1})	$\Delta_r S^{\ominus}_m$ (J mol^{-1} K^{-1})	$\Delta_r G^{\ominus}_m$ (kJ mol^{-1})	*r*
4a-Im	-43.52	-59.75	-25.71	0.9998
4a-*N*-MeIm	-54.30	-86.05	-28.64	0.9999
4b-Im	-52.73	-85.85	-27.13	0.9998
4b-*N*-MeIm	-63.69	-114.94	-29.42	0.9990
4c-Im	-36.82	-36.56	-25.91	0.9998
4c-*N*-MeIm	-38.93	-38.42	-27.48	0.9994

Compared with **4a**, the charge on the Zn atom was larger in **4b** (1.074 e) and smaller in **4c** (1.068 e), which indicates that the Cl substituent increased the charge on the Zn atom and that the methyl group substituent decreased this charge. After Im or *N*-MeIm bonded to **4a**, **4b**, and **4c**, the charge on the Zn atom was reduced, indicating that the coordination reaction has occurred between Im, *N*-MeIm, and Zn porphyrins.

After the coordination reaction, the average Zn-N distance in the porphyrin ring increased; this change was calculated to be from 2.107 to 2.110 Å, which is similar to the Zn-H distances of five-coordinate Zn porphyrins reported in the literature[27]. The bond length for **4b**-*N*-MeIm (2.232 Å) was the shortest and the bond energy for **4b**-*N*-MeIm (66.8 kJ mol^{-1}) was the largest. These findings indicate close bonding between *N*-MeIm and **4b**, consistent with the experimental results.

Fluorescence spectra

The characteristic peaks of the S_1 states of **4a**, **4b**, and **4c** were seen at 597.2 and 645.8 nm, 598.2 and 645.9 nm, and 604.3 and 650.2 nm, respectively. Figure 4 shows the fluorescence spectrum of the **4a**-*N*-MeIm system at room temperature. This reveals that the addition of different concentrations of *N*-MeIm to a fixed concentration of **4a** markedly changed the fluorescence curve of the mixed system, confirming that these molecules reacted with each other. The fluorescent intensity decreased in the presence of increasing concentrations of *N*-MeIm, indicating fluorescence quenching. The N atom formed coordination bonds with Zn^{2+} by a σ bond after coordination. However, Zn^{2+} formed a feedback π bond with the N atom by *d* electrons.

Table 3—The charges on the Zn atoms, Zn-N bond lengths, and bond energies for the studied systems

Porphyrins	Charge on Zn (e)	Bond energy (kJ mol^{-1})	Zn-N bond length (Å)
4a	1.071		
4b	1.074		
4c	1.068		
4a-Im	1.042	61.5	2.244
4b-Im	1.048	64.6	2.239
4c-Im	1.040	60.0	2.246
4a-*N*-MeIm	1.041	63.4	2.236
4b-*N*-MeIm	1.042	66.8	2.232
4c-*N*-MeIm	1.039	61.9	2.238

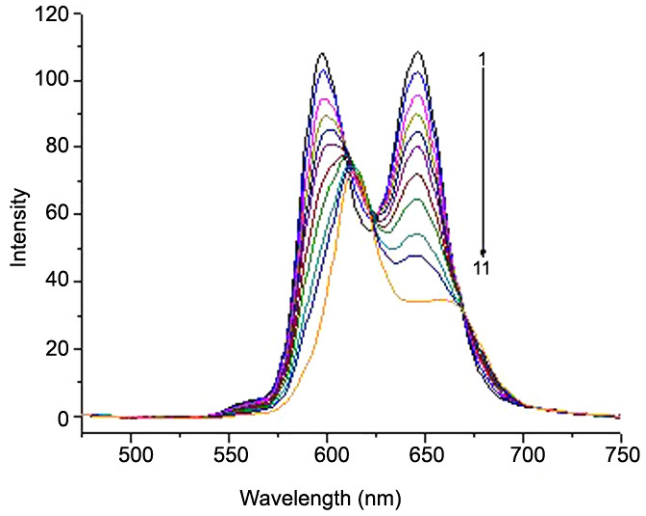

Fig. 4—Fluorescence spectrum of the system of 4a and *N*-MeIm. [Curve 1: 4a, 2.5×10^{-6} mol·L^{-1}; 2-11: $c_{N\text{-MeIm}}$:c_{4a}=2, 4, 6, 8, 10, 15, 20, 30, 40, 100].

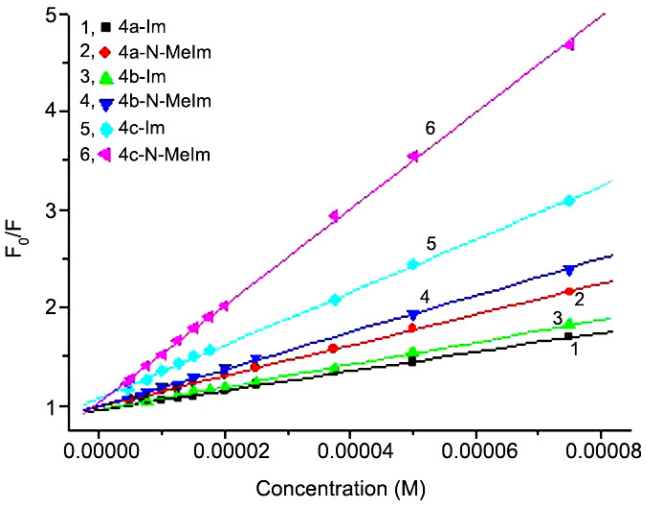

Fig. 5—The Stern-Volmer curves at room temperature.

Since Zn^{2+} had more *d* electrons, the feedback π bond increased the electron density of the porphyrin ring, and the distribution of the electron cloud was more irregular in the entire conjugation system. This changes the vibrational mode of the S_1 state and strengthened the non-radiative transition from S_1 to T_1[42,43]. The same change in fluorescence spectroscopy exists between the other zinc porphyrins and imidazole derivatives.

In order to quantify fluorescence quenching, we obtained the Stern-Volmer quenching rate constant (K_q) by plotting and fitting F_0/F against [*Q*] in the Eq. (4) at room temperature (Fig. 5). These values are shown in Table 4. The values of

Table 4—The quenching rate constant (K_q) at room temperature

Systems	F_0/F~[*Q*]	K_q (L mol^{-1} s^{-1})	*r*
4a-Im	0.9516+9887[*Q*]	$(9.89\pm0.001)\times10^{11}$	0.9996
4a-*N*-MeIm	0.9866+15651[*Q*]	$(1.57\pm0.005)\times10^{12}$	0.9998
4b-Im	0.9567+11435[*Q*]	$(1.14\pm0.006)\times10^{12}$	0.9996
4b-*N*-MeIm	0.9916+18807[*Q*]	$(1.88\pm0.001)\times10^{12}$	0.9995
4c-Im	1.0754+26962[*Q*]	$(2.70+0.004)\times10^{12}$	0.9994
4c-*N*-MeIm	1.0382+49216[*Q*]	$(4.92\pm0.008)\times10^{12}$	0.9996

K_q were all > 2.0×10^{10} L mol^{-1} s^{-1} (the constant of maximum diffusion collision quenching rate), indicating compound formation prior to excitation. The largest K_q value was observed for **4c**-*N*-MeIm.

Conclusions

Three free porphyrins modified using Boc-D-threonine, and their zinc porphyrins were synthesized. The interactions between zinc porphyrins and imidazole derivatives were studied using UV-vis spectroscopy, fluorescence spectra, and quantum chemistry to investigate the effects of peripheral substituents on their coordination reactions. These results indicated that the reaction was spontaneous, with coordinated bonds between zinc porphyrins and imidazole derivatives. The value (*n*), the association constant ($K^{\ominus}$), and the thermodynamic parameters ($\Delta_rG^{\ominus}_m$, $\Delta_rH^{\ominus}_m$, and $\Delta_rS^{\ominus}_m$) were determined at four different temperatures. The study shows that ability to form complexes is related to the peripheral substituents in zinc porphyrins and the structure of the imidazole derivatives. We obtained the bond length, charge, and bond energy for each system by theoretical calculations, which were consistent with experimental values. Different zinc porphyrins and imidazole derivatives altered fluorescence quenching.

Acknowledgement

This work was supported by the Natural Science Foundation of Hebei Province (No. B2014408009), the Key Project of Colleges and Universities in Hebei Province Science and Technology Research (No. ZD20131050), the Key Program Fund of Langfang Teachers University (No. LSZZ201301), and the Undergraduate Training Programs for Innovation and Entrepreneurship in Hebei Province (No. 201410100007).

References

1 Jiang J X, Feng Z Q, Liu B Z, Hu C J & Wang Y, *Dalton Trans*, 42 (2013) 7651.

2 Schmitt J, Heitz V, Sour A, Bolze F, Ftouni H, Nicoud J F, Flamigni L & Ventura B, *Angew Chem Int Ed*, 54 (2015) 169.

3 Tanaka T & Osuka A, *Chem Soc Rev*, 44 (2015) 943.
4 Krüger R A, Terpstra A S & Sutherland T C, *Can J Chem*, 89 (2011) 214.
5 Choi J K, Sargsyan G, Johnson B D & Balaz M, *RSC Adv*, 5 (2015) 15916.
6 Brahma S, Ikbal S A & Rath S P, *Inorg Chem*, 53 (2014) 49.
7 Brahma S, Ikbal S A, Dhamija A & Rath S P, *Inorg Chem*, 53 (2014) 2381.
8 Anyika M, Gholami H, Ashtekar K D, Acho R & Borhan B, *J Am Chem Soc*, 136 (2014) 550.
9 Sainna M A, Kumar S, Kumar D, Fornarini S, Crestoni M E & Visser S P D, *Chem Sci*, 6 (2015) 1516.
10 Benelli T, Angiolini L, Caretti D, Lanzi M, Mazzocchetti L, Salatelli E & Giorgini L, *Dyes Pigments*, 106 (2014) 143.
11 Brahma S, Ikbal S A, Dey S & Rath S P, *Chem Commun*, 48 (2012) 4070.
12 Marets N, Bulach V & Hosseini M W, *New J Chem*, 37 (2013) 3549.
13 Mbouguen J C K & Angnes L, *Sensors Actuators B*, 212 (2015) 464.
14 Maeda C, Taniguchi T, Ogawa K & Ema T, *Angew Chem*, 127 (2015) 136.
15 Angiolini L, Benelli T & Giorgini L, *React Funct Polym*, 71 (2011) 204.
16 Chen S G, Yu Y, Zhao X, Ma Y G, Jiang X K & Li Z T, *J Am Chem Soc*, 133 (2011) 11124.
17 Andernach R E, Rossbauer S, Ashraf R S, Faber H, Anthopoulos T D, McCulloch I, Heeney M & Bronstein H A, *ChemPhysChem*, 16 (2015) 1223.
18 Kamimura T, Komura M, Komiyama H, Iyodac T & Tani F, *Chem Commun*, 51 (2015) 1685.
19 Jiang J X, Fang X S, Liu B Z & Hu C J, *Inorg Chem*, 53 (2014) 3298.
20 O'Brien J A, Lu Y, Hooley E N, Ghiggino K P, Steer R P & Paige M F, *Can J Chem*, 89 (2011) 122.
21 Pintre I C, Pierrefixe S, Hamilton A, Valderrey V, Bo C & Ballester P, *Inorg Chem*, 51 (2012) 4620.
22 Chaudhary A & Rath S P, *Chem Eur J*, 17 (2011) 11478.
23 Gros C P, Brisach F, Meristoudi A, Espinosa E, Guilard R & Harvey P D, *Inorg Chem*, 46 (2007) 125.
24 Borovkov V V, Fujii I, Muranaka A, Hembury G A, Tanaka T, Ceulemans A, Kobayashi N & Inoue Y, *Angew Chem Int Ed*, 43 (2004) 5481.
25 Chaudhary A, Ikbal S A, Brahma S & Rath S P, *Polyhedron*, 52 (2013) 761.
26 Ikbal S A, Brahma S & Rath S P, *Chem Commun,* 51 (2015) 895.
27 Mondal P, Chaudhary A & Rath S P, *Dalton Trans*, 42 (2013) 12381.
28 Maligaspe E, Kumpulainen T, Lemmetyinen H, Tkachenko N V, Subbaiyan N K, Zandler M E & D'Souza F, *J Phys Chem A*, 114 (2010) 268.
29 Yoosaf K, Iehl J, Nierengarten I, Hmadeh M, Gary A M A, Nierengarten J F & Armaroli N, *Chem Eur J*, 20 (2014) 223.
30 Tan Y Y, Escorcia N, Hyslop A & Wang E J, *Anal Chem Res*, 3 (2015) 70.
31 Venditto V J, Watson D S, Motion M, Montefiori D & Szoka F C J, *Clin Vacc Immunol,* 20 (2013) 39.
32 Darbinian N, Khalili K & Amimi S, *J Cell Physiol*, 229 (2014) 153.
33 Harada K, Fujitsuka M, Sugimoto A & Majima T, *J Phys Chem C*, 111 (2007) 11430.
34 Kuroda Y, Kato Y, Higashioji T, Hasegawa J Y, Kawanami S, Takahashi M, Shiraishi N, Tanabe K & Ogoshi H, *J* Am Chem Soc*,* 117 (1995) 10950.
35 Dehghani H & Mansournia M R, *Spectrochim Acta: A*, 74 (2009) 324.
36 Souza F D, Khouly M E E, Gadde S, Mccarty A L, Karr P A, Zandler M E, Araki Y & Ito O, *J Phys Chem B*, 109 (2005) 10107.
37 Becke A D, *J Chem Phys*, 98 (1993) 5648.
38 Zhang L J, Qi D D, Zhang Y X, Bian Y Z & Jiang J Z, *J Mol Graph Modell*, 29 (2011) 717.
39 *Gaussian 09, Rev. A.1,* (Gaussian, Inc., Wallingford CT) 2009.
40 Quezada D, Honores J, Aguirre M J & Isaacs M, *J Coord Chem*, 67 (2014) 4090.
41 Mizutani T, Wada K & Kitagawa S, *J Org Chem*, 65 (2000) 6097.
42 Feng J, Zhang H J, Xiang J F, Ai X C, Zhang X K, Xu G Z & Zhang J P, *Sci China* (*Series B*), 46 (2003) 137.
43 Yagi S, Ezone M, Yonekura I, Takagishi T & Nakazumi H, *J Am Chem Soc*, 125 (2003) 4068.